GENERALIZED NEWTONIAN FLUID CONSTITUTIVE EQUATION FOR POLYMER LIQUIDS CONSIDERING CHAIN STRETCH AND MONOMERIC FRICTION REDUCTION FOR VERY FAST FLOWS MODELING

Martin Zatloukal* and Jiri Drabek

Polymer Centre, Faculty of Technology, Tomas Bata University in Zlín,

Vavrečkova 275, 760 01 Zlín, Czech Republic

Keywords: Polymer rheology, uniaxial extensional flow, chain stretch, monomeric friction reduction, constitutive equations.

*Corresponding author: mzatloukal@utb.cz

ABSTRACT

In this work, the recently proposed frame-invariant Generalized Newtonian Fluid (GNF) constitutive equation [M. Zatloukal, Physics of Fluids 32(9), 091705 (2020)] has been modified to provide uniaxial extensional viscosity at high strain rate limit corresponding to molecular expression for a fully extended Fraenkel chain reported in [G. Ianniruberto, G. Marrucci, and Y. Masubuchi, Macromolecules 53(13), 5023-5033 (2020)]. It uses basic rheological and molecular parameters together with the ratio of monomeric friction coefficients for equilibrium and fully aligned chains. The modified GNF model was successfully tested by using steady-state uniaxial extensional viscosity data for well-characterized entangled polymer melts and solutions (namely linear isotactic polypropylenes, poly(n-butyl acrylate), polyisoprenes and polystyrenes) covering a wide range of strain rates, including those, at which the chain stretch occur. Only two fitting parameters were sufficient to describe all uniaxial extensional viscosity data, one related to the Rouse stretch time and the other controlling the extensional thinning and thickening behavior at medium and high strain rates. The model was compared to five different advanced viscoelastic constitutive equations, which are based on Doi-Edwards theory and include chain stretch along with a number of important additions. The ability of the proposed GNF model to represent steady uniaxial extensional viscosities under fast flow conditions for entangled polymer fluids has been shown to be superior to the predictions of selected advanced viscoelastic constitutive equations. It is believed that the modified GNF model can be used in the stable modeling of non-Newtonian polymer liquids, especially in very fast steady-state flows where chain stretch begins to occur.

INTRODUCTION

Knowledge of polymer melt dynamics and stability at very fast flows (i.e. at high speeds and/or in the small channels where orientational and/or stretch Weissenber number is higher than 1 [1, 2]) is essential for the optimization and development of new polymeric materials used to produce micro/nano-products via advanced technologies such as additive manufacturing (alias 3D printing) [3-8] micromolding [9-13], nano-imprint lithography [14-18], film casting [19-25], meltblown [26-29] and electrospinning [30-32]. It was found that the flow behavior of polymer melts in highly confined geometries is significantly different from those of the bulk [33-35] (i.e. classic Navier-Stokes equations with dimension-independent viscosity are not applicable for modeling purposes), strain rates are very high [36-40] and both, flow facilitation [38, 41-45] (caused by slip, reduced degree of coil-coil interpenetration, viscous dissipation, flow-induced chain scission) as well as flow stiffening [39, 46-49] (due to flow-induced crystallization, melt compressibility, collective molecular motion or molecular immobility at the solid surfaces) can be observed. In recent years, specific attention has been paid to flow-induced chain stretch and monomeric friction coefficients, which control extensional rheology [50-53] and flow-induced crystallization [54-60] in fast flows. Because both of these factors are not currently included in the modeling of industrially important complex flows, the understanding of the dynamics of polymer liquids and their stability is very limited in such cases. This significantly limits the optimization and development of the above-mentioned advanced technologies. There are also a number of constitutive equations with a high ability to describe the extensional rheology of polymeric fluids (such as the molecular stress function (MSF) model [61-64] for entangled polymer melts or the recently proposed constitutive equation Narimissa and Wagner (NW) [65] for disentangled melts), but because they do not consider flow-induced reduction of the monomeric friction coefficient, their molecular basis is unclear, as described, for example, in [51, 66].

The aim of this work is to combine recent knowledge about the dynamics of polymer liquids in very fast uniaxial extensional flows resulting from molecular arguments [52, 67] with the recently proposed frame-invariant formulation of Generalized Newtonian Fluid (GNF) constitutive equation [68], which could be useful for steady-state flow modeling under flow conditions typical for the production of micro/nano-products or products with nanofeatures, where the monomeric friction coefficient can be significantly reduced.

CONSTITUTIVE EQUATION

Frame-invariant Generalized Newtonian Fluid Model with $\eta_\infty \neq 0$

In this work, we used GNF constitutive equation, which belongs to a new family of models [68-73], where the strain rate dependent viscosity $\eta(D)$, is modified as $\eta = A^{1-f}\eta(D)^f$, where the constant A is related to the high-strain rate plateau values of the shear and extensional viscosities and f is function evaluating the intensity of stretching during flow. The models handle the differences between high-extensional-rate uniaxial, planar and biaxial extensional viscosities compared to others, more advanced constitutive equations (including the molecular-based Pom–Pom model), which unrealistically predict steady-state uniaxial and planar extensional viscosities virtually identical at high extensional strain rates [19, 68, 74]. These types of GNF models have been successfully tested for polymer melts with linear (mLLDPE [68, 71], HDPE [68, 69]) and differently branched structures (mLLDPE [68, 69,71], mHDPE [68], LDPE [68-70, 72]) including polymers with star type of the branching (LCB-PP [73]) using steady-state extensional viscosities measured at extensional strain rates typically up to about 10 s^{-1}, (i.e. at low *Wi*, where entanglements dominate the dynamics). In this work, a very recently proposed frame-invariant formulation of the GNF model [68] was used:

$$\sigma = 2\eta\left(II_{\bar{L}}, II_D, III_D\right)D - p\delta, \tag{1}$$

where

$$\eta\left(II_{\bar{L}}, II_D, III_D\right) = A^{1-\mathrm{f}\left(II_{\bar{L}}, II_D, III_D\right)}\eta\left(II_D\right)^{\mathrm{f}\left(II_{\bar{L}}, II_D, III_D\right)}, \tag{2}$$

$$\eta\left(II_D\right) = \eta_\infty + \frac{\eta_0 - \eta_\infty}{\left[1+\left(\lambda_1\sqrt{II_D}\right)^a\right]^{\frac{1-n}{a}}}, \tag{3}$$

$$\mathrm{f}\left(II_{\bar{L}}, II_D, III_D\right) = \left\{\tanh\left[\lambda_2\left(1+\frac{1}{12\sqrt{3}}\right)^{-\psi}\left(\left|1+\frac{III_D}{II_D^{3/2}}\right|\right)^{\psi}\sqrt{II_{\bar{L}}}+\beta\right]\frac{1}{\tanh\left(\beta\right)}\right\}^{\xi}. \tag{4}$$

Here σ is the total stress tensor, p is the pressure, δ is the unit tensor, D represents the strain rate tensor and $\eta\left(II_{\bar{L}}, II_D, III_D\right)$ means the viscosity, which can vary with the second invariant of the objective velocity gradient $II_{\bar{L}} = 2\mathrm{tr}\left(\bar{L}^2\right)$, where $\bar{L}$ and the velocity gradient L are the same in steady-state flows, as well as on the second $II_D = 2\mathrm{tr}\left(D^2\right)$, and third, $III_D = \det\left(D\right)$, invariants of D. The A, η_0, η_∞, λ_1, a, n, λ_2, ψ, β, ξ are adjustable parameters. In the pure shear flow, $II_{\bar{L}} = II_L = 0$ and thus $\mathrm{f}\left(II_{\bar{L}}, II_D, III_D\right)$ becomes equal to 1, i.e. the shear viscosity becomes dependent on the second invariant of the strain rate tensor only with $II_D = \dot{\gamma}^2$ as follows:

$$\eta\left(\dot{\gamma}\right) = \eta_\infty + \frac{\eta_0 - \eta_\infty}{\left[1+\left(\lambda_1\dot{\gamma}\right)^a\right]^{\left(\frac{1-n}{a}\right)}}. \tag{5}$$

Eq. 5 is called the Carreau-Yasuda model, which has the ability to fit a wide range of experimental $\eta\left(\dot{\gamma}\right)$ data for many polymer solutions and melts [75].

For the uniaxial extensional flow, in which $II_{\bar{L}} = II_L = II_D = 3\dot{\varepsilon}^2$, $III_D = \dot{\varepsilon}^3/4$, the function $\mathrm{f}\left(II_{\bar{L}}, II_D, III_D\right)$ given by Eq. 4 simplifies to the following form:

$$\mathrm{f}\left(II_{\bar{L}}, II_D, III_D\right) = \left[\tanh\left(\lambda_2\sqrt{3}\dot{\varepsilon}+\beta\right)/\tanh(\beta)\right]^{\xi} . \quad (6)$$

Combination of Eqs. 1-3 and 6 leads to the following expression for uniaxial extensional viscosity

$$\eta_{E,U}\left(\dot{\varepsilon}\right) = 3A^{1-\left[\tanh\left(\lambda_2\sqrt{3}\dot{\varepsilon}+\beta\right)/\tanh(\beta)\right]^{\xi}} \left\{\eta_\infty + \frac{\eta_0-\eta_\infty}{\left[1+\left(\lambda_1\sqrt{3}\dot{\varepsilon}\right)^a\right]^{\left(\frac{1-n}{a}\right)}}\right\}^{\left[\tanh\left(\lambda_2\sqrt{3}\dot{\varepsilon}+\beta\right)/\tanh(\beta)\right]^{\xi}} . \quad (7)$$

Considering that $\lim_{\dot{\varepsilon}\to\infty}\eta_{E,U}\left(\dot{\varepsilon}\right) = \eta_{E,U,\infty}$, the parameter A can be expressed by the infinite uniaxial extensional viscosity, $\eta_{E,U,\infty}$, as follows

$$A = \left(\frac{\eta_{E,U,\infty}\eta_\infty^{-\alpha}}{3}\right)^{\frac{1}{1-\alpha}}, \quad (8)$$

where

$$\alpha = \left[\tanh\left(\beta\right)\right]^{-\xi}. \quad (9)$$

Here, the parameters η_0, η_∞, λ_1, a, n are determined from the shear viscosity data fitting by the Carreau-Yasuda model (Eq.3), while the parameters β, λ_2, ξ and A are obtained by fitting the uniaxial extensional viscosity data using the Eq. 7. In this case, the parameter ψ disappears.

Molecularization of GNF Model with $\eta_\infty \neq 0$ for entangled polymer melts and solutions

The parameters of the GNF model can be related to the molecular parameters of a given polymer fluid utilizing the Rouse stretch time according to Doi and Edwards (Eq. 10 [76,77]), the Osaki's definition of the Rouse stretch time (Eq. 11 [78]) and the analytical expression for uniaxial extensional viscosity saturating in very fast flows at the constant value, $\eta_{E,U,\infty}$, which was derived for the fully extended Fraenkel chain just recently (Eq. 12 [52, 67]).

$$\tau_R = \frac{N^2 b^2}{3\pi^2 k_B T}\zeta_{eq} \tag{10}$$

$$\tau_R = \frac{12M\eta_0}{\pi^2 \rho\varphi RT}\left[\frac{M_c(\varphi)}{M}\right]^{x-1} \tag{11}$$

$$\eta_{E,U,\infty} = \frac{\nu b^2 N^2}{12}\zeta_{aligned} \tag{12}$$

Here, b the Kuhn segment length, k_B the Boltzmann constant, T is the thermodynamic temperature, ζ_{eq} the equilibrium monomeric friction coefficient, M the molar mass, η_0 the zero-shear rate viscosity, $M_c(\varphi)$ the critical molar mass at which entanglements starts to occur, ρ the density, φ the volume fraction of polymer in solution ($\varphi=1$ for the melt) [79], R the universal gas constant, $\zeta_{aligned}$ the friction coefficient for the fully stretched chain, N and ν are the number of Kuhn segments and the Kuhn segment number density, respectively, defined as

$$N = \frac{M}{M_k}, \tag{13}$$

$$\nu = \frac{\rho N_a}{M_k}. \tag{14}$$

Here, M_k the Kuhn segment molar mass and N_a is the Avogadro number relating R and k_B as $N_a=R/k_B$. Combination of Eqs. 10-12 leads to the following expression for the $\eta_{E,U,\infty}$ normalized by the three times zero-shear viscosity considering here that the zero-shear rate viscosity scales with M^x with x of 3.5 ± 0.2 for all linear and flexible molecules [76] rather than with the fixed value $x=3.4$ [52]

$$\frac{\eta_{E,U,\infty}}{3\eta_0} = \frac{M_c(\varphi)^{x-1}}{M_K}\frac{M^{2-x}}{\varphi}\frac{\zeta_{aligned}}{\zeta_{eq}}. \tag{15}$$

The $M_c(\varphi)$ the critical molar mass at which entanglements starts to occur, which can be calculated based on the Fetters et al. [80] formula using the molar mass between entanglements for the melt, M_e, (defined

according to Ferry as $M_e = \frac{\rho RT}{G_N^0}$ with G_N^0 being the plateau modulus [76]), which is generalized here considering that the molar mass between entanglements for polymer solutions, $M_e(\varphi)$ is given as M_e / φ [79, 81]:

$$M_c(\varphi) = \left(\frac{9.2*10^{-10}}{p}\right)^{0.65} M_e(\varphi) \tag{16}$$

where p is the packing length. The M_k can be determined from the ratio of the number of backbone bonds, n, and N, which is related to the Flory's characteristic ratio C_∞ and the backbone bond angle θ as [82]

$$\frac{n}{N} = \frac{C_\infty}{\cos^2(\theta/2)}, \tag{17}$$

where n can be calculated from Eq. 18 using the average molar mass per backbone bond, m_b, as [82]

$$n = \frac{M}{m_b}. \tag{18}$$

Combination of Eqs. 13, 17-18 leads to the following expression for the M_k:

$$M_k = m_b \frac{C_\infty}{\cos^2(\theta/2)}. \tag{19}$$

Note that the Kuhn segment length, b, appearing in Eqs. 10 and 12, is defined as [82]

$$b = \frac{C_\infty l}{\cos(\theta/2)}, \tag{20}$$

where l is the average backbone bond length ($1.54*10^{-10}$ m for the carbon-carbon bond [83, 84]). For very fast extensional flows ($\dot{\varepsilon} \to \infty$), the GNF model yields the following expression for the normalized asymptotic uniaxial extensional viscosity (by rearranging of Eq. 8):

$$\frac{\eta_{E,U,\infty}}{3\eta_0} = \frac{A^{1-\alpha}\eta_\infty^\alpha}{\eta_0}. \tag{21}$$

Considering that the $\eta_0 = K_1 M^x$ [56] and $\eta_\infty = K_2 M$ [40, 85], Eq. 21 can be rewritten as

$$\frac{\eta_{E,U,\infty}}{3\eta_0} = \frac{A^{1-\alpha} K_2^{\alpha}}{K_1} M^{\alpha - a}. \tag{22}$$

Here, if $\alpha = 2$, the power in *M* becomes equal to $2 - x$, i.e the same as in the Eq.12. In this specific case, it makes it possible to relate the parameter *A* to the ratio of the coefficients of friction derived for a fully extended Fraenkel chain combining Eq.15 and Eq.22 as follows:

$$A = \frac{\eta_\infty^2 M_k}{\eta_0} M_c(\varphi)^{1-x} M^{x-2} \varphi \frac{\zeta_{eq}}{\zeta_{aligned}}. \tag{23}$$

This allows the determination of parameter *A* in the GNF model from sound molecular parameters with a reduced number of adjustable parameters, because ξ parameter must satisfy the following equation to keep the α value equal to 2

$$\xi = -\frac{\log(2)}{\log\left[\tanh(\beta)\right]} \quad \text{or} \quad \text{alternatively } \beta = \operatorname{artanh}\left(2^{-\frac{1}{\xi}}\right). \tag{24}$$

Thus Eqs. 1-4, where *A* and ξ are defined via Eq.23 and Eq.24, respectively, can be considered as the "molecular based GNF model" (mGNF). It can be useful to express the parameter *A* as a function of the maximum stretch ratio characterizing stretching ability of polymer chains (ratio of fully extended chain length to equilibrium polymer chain length), λ_{max}, which is defined for entangled polymer melts and solutions as [86, 87]

$$\lambda_{\max} = \sqrt{\frac{N}{Z}}, \tag{25}$$

where *N* is the number of Kuhn segments and *Z* is the number of entanglements per chain, that is defined as

$$Z = \frac{M}{M_e(\varphi)}. \tag{26}$$

Combination of Eqs. 13, 23, 25-26 leads to the following expression for parameter *A*:

$$A = \frac{\eta_\infty^2}{\eta_0}\frac{M_e(\varphi)}{\lambda_{\max}^2} M_c(\varphi)^{1-x} M^{x-2}\varphi\frac{\zeta_{eq}}{\zeta_{aligned}} \ . \tag{27}$$

It is interesting to note that the use of $\eta_0 = K_1 M^x$ [56] and $\eta_\infty = K_2 M$ [40, 85] in the Eq. 27 leads to the following molar mass independent expression for *A*:

$$A = \frac{K_2^2}{K_1}\frac{M_e(\varphi)}{\lambda_{\max}^2} M_c(\varphi)^{1-x} \varphi\frac{\zeta_{eq}}{\zeta_{aligned}}. \tag{28}$$

To summarize, the proposed mGNF model is simply the original GNF model given by Eqs.1-4, where $A = \frac{3\eta_\infty^2}{\eta_{E,U,\infty}} = \frac{\eta_\infty^2}{\eta_0}\frac{M_e(\varphi)}{\lambda_{\max}^2} M_c(\varphi)^{1-x} M^{x-2}\varphi\frac{\zeta_{eq}}{\zeta_{aligned}}$ and $\xi = -\frac{\log(2)}{\log\left[\tanh(\beta)\right]}$.

As can be seen, the parameter *A* is directly related to three times the ratio of the square of the infinite-shear-rate viscosity and the infinite-uniaxial extensional-rate viscosity.

RESULTS AND DISCUSSION

In order to understand the proposed model behavior in the uniaxial extensional flow, the parameters λ_{max}, $\frac{\zeta_{eq}}{\zeta_{aligned}}$, λ_2 and β were systematically varied, while the other parameters were kept constant. The maximum stretch ratio, λ_{max}, and $\frac{\zeta_{eq}}{\zeta_{aligned}}$ are usually in the order of units/tenths (polymer melts and entangled solutions), and hundreds (dilute unentangled solutions) [50, 53, 86]. Figures 1-2 show that as λ_{max} increases (or $\frac{\zeta_{eq}}{\zeta_{aligned}}$ decreases), the minimum extensional viscosity value increases, shifts to lower orientational Weissenberg numbers Wi (= $\lambda_1\dot{\varepsilon}$), and the slope in the extensional thinning and thickening region decreases and increases, respectively. The observed trends with respect to λ_{max} correspond well

with predictions of well-established models, such as the Finitely Extensible Nonlinear Elastic model using the Peterlin approximation (FENE-P) for dilute solutions of flexible polymers (or unentangled melts) and the Doi-Edwards-Marrucci-Grizzuti tube-model (DEMG) for concentrated solutions and melts where entanglements dominate the dynamics [86]. The FENE-P model includes Brownian forces, frictional forces, elastic/spring and the finite extensibility, while the DEMG model also captures the reptation with stretch relaxation [86]. The observed trends relating friction in between chains undergoing uniaxial extensional deformation to macroscopic properties (i.e. viscosity thickening and thinning) are in good agreement with recent experimental and theoretical finding on dynamics of polymer liquids in fast flows [50, 52]. The effect of parameters λ_2 and β on the extensional viscosity is shown in Figures 3-4 for two different $\frac{\zeta_{eq}}{\zeta_{aligned}}$ values. As can be seen, these parameters control the extensional thinning and thickening behavior at low and high Wi without changing the $\eta_{E,U,\infty}$ and their effect on the extensional viscosity curve is more dominant at lower $\frac{\zeta_{eq}}{\zeta_{aligned}}$ ratios. In more detail, the extensional thickening at low Wi increases as λ_2 increases or as β decreases. In order to test the proposed mGNF model, strain rate dependent uniaxial viscosity data taken from the open literature for linear isotactic polypropylene (iPP) melts [28, 29, 53], poly(n-butyl acrylate) (PnBA) melt [87], polyisoprene (PI) melt and entangled solutions [87], and polystyrene (PS) entangled solutions [88] were used. For iPP melts, all Carreau-Yasuda model parameters (η_0, η_∞, λ_1, a, n) were taken from [40] and are summarized in Table I. In the case of PnBA, PI, PS entangled liquids, only η_0 and λ_1 are known from the open literature (considering that λ_1 is equal to the reptation relaxation time, τ_d), and thus, it is assumed that firstly, $n = 0$ and $\eta_\infty = 0.02\eta_0$, as for iPPs, and secondly, the shear viscosity can be sufficiently described by a simpler Carreau model [89], i.e. that $a = 2$). The extensional viscosity parameter A was calculated using the Eq. 27 for all samples using basic rheological and molecular parameters (namely η_∞, η_0, $M_e(\varphi)$, λ_{max}, $M_c(\varphi)$,

x, M,φ and $\zeta_{eq}/\zeta_{aligned}$), which are summarized in Tables I-III. Only 2 parameters (λ_2 and β) were used to fit the measured uniaxial extensional viscosity data and their values are summarized in Table IV (where ξ was calculated from β using Eq. 24). It can be seen from Figures 5-7 that the mGNF model has a very high ability to fit the measured data for all tested entangled polymer liquids (including high strain rate data where chain stretch occurs), although the $\zeta_{eq}/\zeta_{aligned}$ values vary considerably. Interestingly, if the obtained fitting parameter λ_2 is plotted against the Rouse stretch time, τ_R, for each tested sample, it was found that the following simple equation can be used to fit this data (see Figure 8):

$$\lambda_2 = \exp\left[0.0697 \ln^2\left(\tau_R\right) + 2.0868 \ln\left(\tau_R\right)\right]. \tag{29}$$

This suggests that the mGNF model parameter λ_2 can be considered as a molecular parameter related to the Rouse stretch time. On the other hand, the second β parameter, which is dimensionless, could be associated with the ratio of the rate of destruction and the creation of the entanglements because it controls the extensional thinning and thickening behavior at W_i numbers where entanglements dominate the dynamics.

In Figure 9, the proposed mGNF model is compared with the best predictions of the following advanced viscoelastic constitutive equations, which are available in the open literature for entangled PS solutions. The first, the Basic DEMG model [88], which includes the chain stretch mechanism according to Marrucci and Grizzutti [90, 91] and the finite extensibility of the form introduced by Mead and Leal [92] and Mead et al. [93]. The second, DEMG/Milner-McLeish CLF model [88], which is the Basic DEMG model with incorporated contour length fluctuations (CLF) according to Milner and McLeish [94]. The third, MLD/Doi-Kuzuu CLF model [88], which is the Mead-Larson-Doi (MLD) model [95] including the Doi-Kuzuu version of the CLF [96, 97]. The fourth, double constraint release model with chain

stretch (DCR-CS) proposed by Ianniruberto and Marrucci [98], which includes double reptation, convective removal of constraints in fast flows and chain stretching. The fifth, DEMG-F(SS) model [99], which is a modified DEMG model involving a decrease in segmental friction, based on the work of Yaoita et al. [100]. As can be seen, the ability of the proposed mGNF model to represent uniaxial extensional viscosity under fast flow conditions for given polymeric liquids is better compared to the predictions of chosen advanced viscoelastic constitutive equations.

In mixed shear and extensional flows, D and $\overline{L}$ have the following form

$$D=\begin{pmatrix} \dot{\varepsilon}_{11} & \frac{\dot{\gamma}}{2} & 0 \\ \frac{\dot{\gamma}}{2} & \dot{\varepsilon}_{22} & 0 \\ 0 & 0 & \dot{\varepsilon}_{33} \end{pmatrix}, \qquad \overline{L}=L=\begin{pmatrix} \dot{\varepsilon}_{11} & \dot{\gamma} & 0 \\ 0 & \dot{\varepsilon}_{22} & 0 \\ 0 & 0 & \dot{\varepsilon}_{33} \end{pmatrix}, \tag{30}$$

which yields

$$II_{\overline{L}}=2tr\left(\overline{L}^2\right)=2\dot{\varepsilon}_{11}^2+2\dot{\varepsilon}_{22}^2+2\dot{\varepsilon}_{22}^3, \tag{31}$$

$$II_D=2tr\left(D^2\right)=\dot{\gamma}^2+2\dot{\varepsilon}_{11}^2+2\dot{\varepsilon}_{22}^2+2\dot{\varepsilon}_{22}^3, \tag{32}$$

$$III_D=\det\left(D\right)=\dot{\varepsilon}_{11}\dot{\varepsilon}_{22}\dot{\varepsilon}_{33}-\frac{1}{4}\dot{\gamma}^2\dot{\varepsilon}_{33}. \tag{33}$$

Thus, even in this complex case, the mGNF model (combining Eqs. 31-33, 1-4) provides analytical expressions for all components of the total stress tensor. Analytical equations defining equibiaxial and planar extensional viscosities are given in our previous work (Eqs. 10-11 in [68]).

The key advantages of the mGNF model over fully viscoelastic models can be summarized as follows:

- Provides analytical solutions for stress tensor components even in mixed shear and extensional flows. This greatly simplifies steady-state flow modeling, especially for fast flows where other constitutive equations may fail.
- Provides analytical solutions for shear and especially for uniaxial, planar and biaxial extensional viscosities. This makes the identification of model parameters simple.
- The mGNF model handles differences between high-extensional-rate uniaxial, planar and biaxial extensional viscosities using the parameter ψ compared to other more advanced constitutive equations, which unrealistically predict steady-state uniaxial and planar extensional viscosities virtually identical at high extensional strain rates.
- mGNF model can provide a much better ability to describe steady-state uniaxial extensional viscosities in fast flows than advanced viscoelastic constitutive equations.

On the other hand, the mGNF is not viscoelastic. Thus, it cannot handle the basic features of viscoelastic liquids, such as time-dependent stress (i.e. transient responses), fluid memory, and non-zero values of the first and second normal stress differences.

CONCLUSION

In this work, the recently proposed frame-invariant GNF model [68] was modified to match the expression for normalized uniaxial extensional viscosity at high strain rate limit by the zero-shear viscosity using recent results for a fully extended Fraenkel chain [52, 67] and the Rouse stretch time defined by Doi and Edwards [76, 77] and Osaki [78]. In general, the mGNF model uses a total of 9 parameters that needs to be identified using shear (η_0, η_∞, λ_1, a and n), uniaxial (A, λ_2 and β) and planar/biaxial (ψ) extensional viscosity data. It has been shown that the parameter A can be calculated directly from the basic rheological (η_0, η_∞) and molecular (M_e, λ_{max}, M_c, M, x and $\zeta_{eq}/\zeta_{aligned}$)

characteristics, if available, and the number of fitting parameters can be therefore further reduced. The performed parametric study showed that mGNF predictions for strain-rate dependent uniaxial extensional viscosity data show comparable trends as prediction of well-established models such as FENE-P and tube-model (DEMG). The proposed model was tested using strain rate dependent uniaxial viscosity data taken from the open literature for well-characterized entangled polymer melts and solutions (iPP, PnBA, PI and PS) whose molecular characteristics were available in the open literature (or were calculated from these data). Only 2 fitting parameters (λ_2 and β) were used to fit the experimental data keeping all other parameters fixed. It was found that the proposed mGNF model is able to fit uniaxial extensional viscosities, including a very high deformation rate range. It was shown that the parameter λ_2 is related to the Rouse stretch time and the non-linear parameter β controls the extensional thinning and thickening behavior at medium and high strain rates without changing the $\eta_{E,U,\infty}$. The proposed mGNF model was compared with five different advanced viscoelastic constitutive equations, which are based on Doi-Edwards theory and include chain stretch along with a number of important additions (namely Basic DEMG, DEMG/Milner-McLeish CLF, MLD/Doi-Kuzuu CLF, DCR-CS, DEMG-F(SS)). It was shown that the ability of the mGNF model to represent steady-state uniaxial extensional viscosities under fast flow conditions for given polymeric liquids is much better compared to the predictions of chosen advanced viscoelastic constitutive equations. It is believed that the proposed mGNF model can be used for stable modeling of non-Newtonian polymer liquids, especially in strong extensional flows, where chain stretch begins to occur. The mGNF model can also be considered a good candidate for modeling advanced polymer processing where high strain rates are achieved (such as the production of energy storage membranes [101, 102] or nanofibers using the melt blown technology [26, 27]), as it provides simple analytical expressions for all components of the stress tensor even in complex flows.

ACKNOWLEDGMENTS

The authors wish to acknowledge Grant Agency of the Czech Republic (Grant registration No. 21-09174S) for the financial support.

DATA AVAILABILITY

The data that support the findings of this study are available within the article.

REFERENCES

1. Y. Matsumiya, H. Watanabe, "Non-Universal Features in Uniaxially Extensional Rheology of Linear Polymer Melts and Concentrated Solutions: A Review," Progress in Polymer Science, **112**, art. no. 101325 (2021).
2. R.G. Larson, P.S. Desai, "Modeling the rheology of polymer melts and solutions," Annual Review of Fluid Mechanics, **47**, 47-65 (2015).
3. D. Vaes, P. Van Puyvelde, "Semi-crystalline feedstock for filament-based 3D printing of polymers," Progress in Polymer Science, **118**, art. no. 101411 (2021).
4. C.M. González-Henríquez, M.A. Sarabia-Vallejos, J. Rodriguez-Hernandez, "Polymers for additive manufacturing and 4D-printing: Materials, methodologies, and biomedical applications," Progress in Polymer Science, **94**, 57-116 (2019).
5. S.C. Ligon, R. Liska, J. Stampfl, M. Gurr, R. Mülhaupt, "Polymers for 3D Printing and Customized Additive Manufacturing," Chemical Reviews, **117**(15), 10212-10290 (2017).
6. Z. Ouyang, E. Bertevas, D. Wang, B.C. Khoo, J. Férec, G. Ausias, N. Phan-Thien, "A smoothed particle hydrodynamics study of a non-isothermal and thermally anisotropic fused deposition modeling process for a fiber-filled composite," Physics of Fluids, **32**(5), art. no. 053106 (2020).
7. Z. Ouyang, E. Bertevas, L. Parc, B.C. Khoo, N. Phan-Thien, J. Férec, G. Ausias, "A smoothed particle hydrodynamics simulation of fiber-filled composites in a non-isothermal three-dimensional printing process," Physics of Fluids, **31**(12), art. no. 123102 (2019).
8. E. Bertevas, J. Férec, B.C. Khoo, G. Ausias, N. Phan-Thien, "Smoothed particle hydrodynamics (SPH) modeling of fiber orientation in a 3D printing process," Physics of Fluids, 30(10), art. no. 103103 (2018).

9. K. Maghsoudi, R. Jafari, G. Momen, M. Farzaneh, "Micro-nanostructured polymer surfaces using injection molding: A review," Materials Today Communications, **13**, 126-143 (2017).
10. C. Yang, X.-H. Yin, G.-M. Cheng, "Microinjection molding of microsystem components: New aspects in improving performance," Journal of Micromechanics and Microengineering, **23**(9), art. no. 093001 (2013).
11. U.M. Attia, S. Marson, J.R. Alcock, "Micro-injection moulding of polymer microfluidic devices," Microfluidics and Nanofluidics, **7**(1), 1-28 (2009).
12. J.K. Oh, R. Drumright, D.J. Siegwart, K. Matyjaszewski, "The development of microgels/nanogels for drug delivery applications," Progress in Polymer Science, **33**(4), 448-477 (2008).
13. J. Giboz, T. Copponnex, P. Mélé, "Microinjection molding of thermoplastic polymers: A review," Journal of Micromechanics and Microengineering, **17**(6), art. no. R02, R96-R109 (2007).
14. L.J. Guo, "Nanoimprint lithography: Methods and material requirements," Advanced Materials, **19**(4), 495-513 (2007).
15. B.D. Gates, Q. Xu, M. Stewart, D. Ryan, C.G. Willson, G.M. Whitesides, "New approaches to nanofabrication: Molding, printing, and other techniques," (2005) Chemical Reviews, **105**(4), 1171-1196.
16. S.Y. Chou, P.R. Krauss, P.J. Renstrom, "Imprint lithography with 25-nanometer resolution," Science, **272**(5258), 85-87 (1996).
17. L.J. Guo, "Recent progress in nanoimprint technology and its applications," Journal of Physics D: Applied Physics, **37**(11), R123-R141 (2004).
18. D. Bratton, D. Yang, J. Dai, C.K. Ober, "Recent progress in high resolution lithography," Polymers for Advanced Technologies, **17**(2), 94-103 (2006).

19. T. Barborik, M. Zatloukal, "Steady-state modeling of extrusion cast film process, neck-in phenomenon, and related experimental research: A review," Physics of Fluids, **32**(6), art. no. 061302 (2020).
20. T. Barborik, M. Zatloukal, "Effect of heat transfer coefficient, draw ratio, and die exit temperature on the production of flat polypropylene membranes," Physics of Fluids, **31**(5), art. no. 053101 (2019).
21. T. Barborik, M. Zatloukal, "Effect of die exit stress state, Deborah number, uniaxial and planar extensional rheology on the neck-in phenomenon in polymeric flat film production," Journal of Non-Newtonian Fluid Mechanics, 255, 39-56 (2018).
22. T. Barborik, M. Zatloukal, C. Tzoganakis, "On the role of extensional rheology and Deborah number on the neck-in phenomenon during flat film casting," International Journal of Heat and Mass Transfer, **111**, 1296-1313 (2017).
23. T. Kanai, G.A. Campbell, *Film Processing Advances* (Hanser Publishers, Munich, 2014).
24. T. Kanai, G.A. Campbell, *Film Processing* (Hanser Publishers, Munich, 1999).
25. B.A. Morris, *The Science and Technology of Flexible Packaging: Multilayer Films from Resin and Process to End Use* (Elsevier, Amsterdam, 2017).
26. J. Drabek, M. Zatloukal, "Meltblown technology for production of polymeric microfibers/nanofibers: A review," Physics of Fluids, **31**(9), art. no. 091301 (2019).
27. Y. Kara, K. Molnár "A review of processing strategies to generate melt-blown nano/microfiber mats for high-efficiency filtration applications," Journal of Industrial Textiles (2021), https://doi.org/10.1177/15280837211019488
28. J. Drabek, M. Zatloukal, "Influence of molecular weight, temperature, extensional rheology on melt blowing process stability for linear isotactic polypropylene," Physics of Fluids, **32**(8), art. no. 083110 (2020).

29. J. Drabek, M. Zatloukal, "Influence of long chain branching on fiber diameter distribution for polypropylene nonwovens produced by melt blown process," Journal of Rheology, **63**(4), 519-532 (2019).
30. J. Xue, T. Wu, Y. Dai, Y. Xia, "Electrospinning and electrospun nanofibers: Methods, materials, and applications," Chemical Reviews, **119**(8), 5298-5415 (2019).
31. T.D. Brown, P.D. Dalton, D.W. Hutmacher, "Melt electrospinning today: An opportune time for an emerging polymer process," Progress in Polymer Science, **56**, 116-166 (2016).
32. E. Loccufier, J. Geltmeyer, L. Daelemans, D.R. D'hooge, K. De Buysser, K. De Clerck, "Silica Nanofibrous Membranes for the Separation of Heterogeneous Azeotropes," Advanced Functional Materials, **28**(44), art. no. 1804138 (2018).
33. H.D. Rowland, W.P. King, J.B. Pethica, G.L.W. Cross, "Molecular confinement accelerates deformation of entangled polymers during squeeze flow," Science, **322** (5902), 720-724 (2008).
34. C.L. Soles, Y. Ding, "Materials science: Nanoscale polymer processing," Science, **322** (5902), 689-690 (2008).
35. S.J. Coombs, A.J. Giacomin, R. Pasquino, "Confinement and complex viscosity," Physics of Fluids, **33**, 053104 (2021).
36. B.R. Whiteside, M.T. Martyn, P.D. Coates, P.S. Allan, Hornsby, G. Greenway, "Micromoulding: Process characteristics and product properties," Plastics, Rubber and Composites, **32**(6), 231-239 (2003).
37. C.J. Ellison, A. Phatak, D.W. Giles, C.W. Macosko, F.S. Bates, "Melt blown nanofibers: Fiber diameter distributions and onset of fiber breakup," Polymer, **48**(11), 3306-3316 (2007).
38. H. Takahashi, T. Matsuoka, T. Kurauchi, "Rheology of polymer melts in high shear rate," Journal of Applied Polymer Science, **30**(12), 4669-4684 (1985).

39. A.L. Kelly, A.T. Gough, B.R. Whiteside, P.D. Coates, "High shear strain rate rheometry of polymer melts," Journal of Applied Polymer Science, **114**(2), 864-873 (2009).
40. J. Drabek, M. Zatloukal, M. Martyn, "Effect of molecular weight on secondary Newtonian plateau at high shear rates for linear isotactic melt blown polypropylenes," Journal of Non-Newtonian Fluid Mechanics, **251**, 107-118 (2018).
41. D. Yao, B. Kim, "Simulation of the filling process in micro channels for polymeric materials," Journal of Micromechanics and Microengineering, **12**(5), 604-610 (2002).
42. R.D. Chien, W.R. Jong, S.C. Chen, "Study on rheological behavior of polymer melt flowing through micro-channels considering the wall-slip effect," Journal of Micromechanics and Microengineering, **15**(8), 1389-1396 (2005).
43. C.S. Chen, S.C. Chen, W.L. Liaw, R.D. Chien, "Rheological behavior of POM polymer melt flowing through micro-channels," European Polymer Journal, **44**(6), 1891-1898 (2008).
44. S.C. Chen, R.I. Tsai, R.D. Chien, T.K. Lin, "Preliminary study of polymer melt rheological behavior flowing through micro-channels," International Communications in Heat and Mass Transfer, **32**(3-4), 501-510 (2005).
45. S. Akkoyun, C. Barrès, Y. Béreaux, B. Blottière, J.Y. Charmeau, "Experimental and numerical investigation of pressure-driven microscale flows of polymer melts: New approach," Journal of Rheology, **58**(2), 467-492 (2014).
46. D. Yao, B. Kim, "Simulation of the filling process in micro channels for polymeric materials," Journal of Micromechanics and Microengineering, **12**(5), 604-610 (2002).
47. A. Cemal Eringen, K. Okada, "A lubrication theory for fluids with microstructure," International Journal of Engineering Science, 33(15), 2297-2308 (1995).
48. J.N. Israelachvili, "Measurement of the viscosity of liquids in very thin films," Journal of Colloid And Interface Science, **110**(1), 263-271 (1986).

49. M.L. Forcada, C.M. Mate, "The Flow of Thin Viscous Liquid Films on Rotating Disks," Journal of Colloid And Interface Science, **160**(1), 218-225 (1993).

50. Y. Matsumiya, H. Watanabe, "Non-Universal Features in Uniaxially Extensional Rheology of Linear Polymer Melts and Concentrated Solutions: A Review," Progress in Polymer Science, **112**, art. no. 101325 (2021).

51. H. Watanabe, Y. Matsumiya, T. Sato, "Revisiting Nonlinear Flow Behavior of Rouse Chain: Roles of FENE, Friction-Reduction, and Brownian Force Intensity Variation," Macromolecules, **54**(8), 3700-3715 (2021).

52. G. Ianniruberto, G. Marrucci, Y. Masubuchi, "Melts of Linear Polymers in Fast Flows," Macromolecules, **53**(13), 5023-5033 (2020).

53. M. Zatloukal, J. Drabek, "Reduction of monomeric friction coefficient for linear isotactic polypropylene melts in very fast uniaxial extensional flow," Physics of Fluids, **33**(5), art. no. 051703 (2021).

54. J. van Meerveld, "A method to extract the monomer friction coefficient from the linear viscoelastic behavior of linear, entangled polymer melts," Rheologica Acta, **43**(6), 615-623 (2004).

55. K. Cui, Z. Ma, N. Tian, F. Su, D. Liu, L. Li, "Multiscale and Multistep Ordering of Flow-Induced Nucleation of Polymers," Chemical Reviews, **118**(4), 1840-1886 (2018).

56. Z. Wang, Z. Ma, L. Li, "Flow-Induced Crystallization of Polymers: Molecular and Thermodynamic Considerations," Macromolecules, **49**(5), 1505-1517 (2016).

57. R.H. Somani, L. Yang, L. Zhu, B.S. Hsiao, "Flow-induced shish-kebab precursor structures in entangled polymer melts," Polymer, **46**(20), 8587-8623 (2005).

58. Pantani, R., Coccorullo, I., Speranza, V., Titomanlio, G. "Modeling of morphology evolution in the injection molding process of thermoplastic polymers," Progress in Polymer Science, **30**(12), 1185-1222 (2005).

59. A.K. Doufas, A.J. McHugh, C. Miller, "Simulation of melt spinning including flow-induced crystallization Part I. Model development and predictions," Journal of Non-Newtonian Fluid Mechanics, **92**(1), 27-66 (2000).

60. R.S. Graham, "Understanding flow-induced crystallization in polymers: A perspective on the role of molecular simulations," Journal of Rheology, **63**(1), 203-214 (2019).

61. M.H. Wagner, S. Kheirandish, O. Hassager, "Quantitative prediction of transient and steady-state elongational viscosity of nearly monodisperse polystyrene melts," Journal of Rheology, **49**(6), 1317-1327 (2005).

62. M.H. Wagner, V.H. Rolón-Garrido, J.K. Nielsen, H.K. Rasmussen, O. Hassager, "A constitutive analysis of transient and steady-state elongational viscosities of bidisperse polystyrene blends," Journal of Rheology, **52**(1), 67-86 (2008).

63. E. Narimissa, M.H. Wagner, "Review on tube model based constitutive equations for polydisperse linear and long-chain branched polymer melts," Journal of Rheology, **63**(2), 361-375 (2019).

64. E. Narimissa, Q. Huang, M.H. Wagner, "Elongational rheology of polystyrene melts and solutions: Concentration dependence of the interchain tube pressure effect," Journal of Rheology, **64**(1), 95-110 (2020).

65. E. Narimissa, M.H. Wagner, "Modeling nonlinear rheology of unentangled polymer melts based on a single integral constitutive equation," Journal of Rheology, **64**(1), 129-140 (2020).

66. T. Sato, Y. Kwon, Y. Matsumiya, H. Watanabe, "A constitutive equation for Rouse model modified for variations of spring stiffness, bead friction, and Brownian force intensity under flow," Physics of Fluids, **33** (6), art. no. 063106, (2021).

67. G. Ianniruberto, G. Marrucci, "Molecular Dynamics Reveals a Dramatic Drop of the Friction Coefficient in Fast Flows of Polymer Melts," Macromolecules, **53**(7), 2627-2633 (2020).

68. M. Zatloukal, "Frame-invariant formulation of novel generalized Newtonian fluid constitutive equation for polymer melts," Physics of Fluids, **32**(9), art. no. 091705 (2020).

69. M. Zatloukal, "A simple phenomenological non-Newtonian fluid model," Journal of Non-Newtonian Fluid Mechanics, **165**(11-12), 592-595 (2010).

70. M. Zatloukal, "Novel non-Newtonian fluid model for polymer melts," Annual Technical Conference - ANTEC, Conference Proceedings, 1, 92-96 (2011).

71. R. Kolarik, M. Zatloukal, M. Martyn, "The effect of polyolefin extensional rheology on non-isothermal film blowing process stability," International Journal of Heat and Mass Transfer, **56**(1-2), 694-708 (2013).

72. M. Zatloukal, "Measurements and modeling of temperature-strain rate dependent uniaxial and planar extensional viscosities for branched LDPE polymer melt," *Polymer*, **104**, 258-267 (2016).

73. J. Drabek, M. Zatloukal, "Evaluation of thermally induced degradation of branched polypropylene by using rheology and different constitutive equations," *Polymers*, **8**(9), art. no. 317 (2016).

74. D. Auhl, D. M. Hoyle, D. Hassell, T. D. Lord, O. G. Harlen, M. R. Mackley, and T. C. B. McLeish, "Cross-slot extensional rheometry and the steady-state extensional response of long chain branched polymer melts," Journal of Rheology 55 (4), 875 (2011)

75. R. B. Bird, R. C. Armstrong, and O. Hassager, *Dynamics of Polymeric Liquids*, 2nd ed. (Wiley, 1987), Vol. **1**.

76. J. M. Dealy, D. J. Read, and R. G. Larson, *Structure and rheology of molten polymers: from structure to flow behavior and back again*, 2nd ed. (Hanser, Munich 2018).

77. M. Doi, and S. F. Edwards, *The Theory of Polymer Dynamics* (Oxford science publications Oxford: Clarendon Press, 1986).

78. K. Osaki, K. Nishizawa, and M. Kurata, "Material Time Constant Characterizing the Nonlinear Viscoelasticity of Entangled Polymeric Systems," Macromolecules, **15**(4), 1068-1071 (1982).

79. M.H. Wagner, E. Narimissa, and Q. Huang, "Scaling relations for brittle fracture of entangled polystyrene melts and solutions in elongational flow," Journal of Rheology, **65**(3), 311-324 (2021).

80. L.J. Fetters, D.J. Lohse, S.T. Milner, and W.W. Graessley, "Packing length influence in linear polymer melts on the entanglement, critical, and reptation molecular weights," Macromolecules, **32**(20), 6847-6851 (1999).

81. Q. Huang, O. Mednova, H. K. Rasmussen, N. J. Alvarez, A. L. Skov, K. Almdal, and O. Hassager, "Concentrated polymer solutions are different from melts: Role of entanglement molecular weight," Macromolecules **46**, 5026–5035 (2013).

82. L. J. Fetters, D. J. Lohse, and R. Colby, "Chain Dimensions and Entanglement Spacings," in *Physical Properties of Polymers Handbook*, 2nd ed., edited by J. E. Mark (Springer, New York, 2007), pp. 447–454.

83. Lide, D.R., *CRC Handbook of Chemistry and Physics*, 84th ed. (CRC Press, Boca Raton, 1999).

84. S. Wu "Control of intrinsic brittleness and toughness of polymers and blends by chemical structure: A review," Polymer International, **29**(3), 229-247 (1992).

85. J. Drabek, M. Zatloukal, M. Martyn, "Effect of molecular weight, branching and temperature on dynamics of polypropylene melts at very high shear rates," Polymer, **144**, 179-183 (2018).
86. R.G. Larson, P.S. Desai, "Modeling the rheology of polymer melts and solutions," Annual Review of Fluid Mechanics, **47**, 47-65 (2015).
87. T. Sridhar, M. Acharya, D.A. Nguyen, P.K. Bhattacharjee, "On the extensional rheology of polymer melts and concentrated solutions," Macromolecules, **47**(1), 379-386 (2014).
88. P.K. Bhattacharjee, J.P. Oberhauser, G.H. McKinley, L.G. Leal, T. Sridhar, "Extensional rheometry of entangled solutions," Macromolecules, **35**(27), 10131-10148 (2002).
89. P. J. Carreau, "Rheological Equations From Molecular Network Theories," Trans Soc Rheol, **16**(1), 99-127 (1972).
90. G. Marrucci, N. Grizzuti, "Fast flows of concentrated polymers: Predictions of the tube model on chain stretching," Gazzetta Chimica Italiana, **118**, 179-185 (1988).
91. D. Pearson, E. Herbolzheimer, N. Grizzuti, G. Marrucci, "Transient behavior of entangled polymers at high shear rates," Journal of Polymer Science Part B: Polymer Physics, **29**(13), 1589-1597 (1991).
92. D.W. Mead, L.G. Leal, "The reptation model with segmental stretch - I. Basic equations and general properties," Rheologica Acta, **34**(4), 339-359 (1995).
93. D.W. Mead, D. Yavich, L.G. Leal, "The reptation model with segmental stretch - II. Steady flow properties," Rheologica Acta, **34**(4), 360-383 (1995).
94. S.T. Milner, T.C.B. Mc Leish, "Reptation and contour-length fluctuations in melts of linear polymers," Physical Review Letters, **81**(3), 725-728 (1998).
95. D.W. Mead, R.G. Larson, M. Doi, "A molecular theory for fast flows of entangled polymers," Macromolecules, **31**(22), 7895-7914 (1998).

96. M. Doi, "Explanation for the 3.4-power law for viscosity of polymeric liquids on the basis of the tube model," Journal of polymer science. Part A-2, Polymer physics, **21**(5), 667-684 (1983).

97. M. Doi, N.Y. Kuzuu, "Rheology of star polymers in concentrated solutions and melts," Journal of Polymer Science: Polymer Letters Edition, **18**, 775– 780 (1980).

98. G. Ianniruberto, G. Marrucci, "A simple constitutive equation for entangled polymers with chain stretch," Journal of Rheology, **45**(6), 1305-1318 (2001).

99. P.S. Desai, R.G. Larson, "Constitutive model that shows extension thickening for entangled solutions and extension thinning for melts," Journal of Rheology, **58**(1), 255-279 (2014).

100. T. Yaoita, T. Isaki, Y. Masubuchi, H. Watanabe, G. Ianniruberto, G. Marrucci, "Primitive chain network simulation of elongational flows of entangled linear chains: Stretch/orientation-induced reduction of monomeric friction" Macromolecules, **45**(6), 2773-2782 (2012).

101. M.K. Purkait, K. Mihir, M. K. Sinha, P. Mondal, and R. Singh, *Stimuli Responsive Polymeric Membranes: Smart Polymeric Membranes* (Academic Press, an imprint of Elsevier, London, 2018).

102. P. Arora, and Z. Zhang, "Battery separators," Chemical Reviews **104**(10), 4419-4462 (2004).

103. Y. Masubuchi, Y. Matsumiya, H. Watanabe, "Test of orientation/stretch-induced reduction of friction via primitive chain network simulations for polystyrene, polyisoprene, and poly(n -butyl acrylate)," Macromolecules, **47**(19), 6768-6775 (2014).

104. P.K. Bhattacharjee, D.A. Nguyen, G.H. McKinley, T. Sridhar, "Extensional stress growth and stress relaxation in entangled polymer solutions," Journal of Rheology, **47**(1), 269-290 (2003).

TABLE I. Carraeu-Yasuda model parameters (Eq. 3) for all samples tested. Values were taken from [28-29, 40, 85] (iPPs), [87] (PnBA and PI) and [88] (PS). Since η_∞, a, λ_1 and n are not available for PnBA, PI and PS liquids, it is considered here that $a = 2$ (in this case the Carreau-Yasuda model becomes a simpler Carreau model), $\eta_\infty = 0.02\eta_0$ and $n = 0$, i.e. similarly to the iPPs.

Sample name	η_0 (Pa.s)	η_∞ (Pa.s)	λ_1 (s)	a (-)	n (-)
iPP 76K	22.80	0.229	0.000222	0.71466	0
iPP 64K	11.27	0.199	0.000101	0.64410	0
iPP 56K	7.79	0.165	0.000070	0.66642	0
PnBA 210K	32800	$0.02\eta_0$	0.79[a]	2	0
PI 145K	60000	$0.02\eta_0$	0.43[a]	2	0
PI 349K 40 wt%	15000	$0.02\eta_0$	0.72[a]	2	0
PI 1M 14 wt%	1000	$0.02\eta_0$	0.43[a]	2	0
PS 10.2M 6.0 wt%	9560	$0.02\eta_0$	39.6[a]	2	0
PS 3.9M 10.0 wt%	4570	$0.02\eta_0$	4.1[a]	2	0

[a] λ_1 is considered to be the same as the reptation relaxation time, τ_d.

TABLE II. Molecular characteristics for all samples taken from [82].

Sample name	ρ (kg/m^3)	p (m)	φ (-)	$M_e(\varphi)$ (kg/mol)	$M_c(\varphi)$[e] (kg/mol)	M_k (kg/mol)	b (m)	$\zeta_{eq}/\zeta_{aligned}$ (-)
iPP 76K	766	$3.12*10^{-10}$	1	6.850	13.935[f]	0.1878	$11.4*10^{-10}$	5.0[k]
iPP 64K	766	$3.12*10^{-10}$	1	6.850	13.935[f]	0.1878	$11.4*10^{-10}$	3.2[k]
iPP 56K	766	$3.12*10^{-10}$	1	6.850	13.935[f]	0.1878	$11.4*10^{-10}$	2.9[k]
PnBA 210K	1080[a]	$3.48*10^{-10}$[b]	1	16.000	30.099	0.948[g]	$18.9*10^{-10}$[i]	1.0[l]
PI 145K	900[a]	$3.13*10^{-10}$	1	6.350	12.798	0.1365	$8.98*10^{-10}$	7.3[l]
PI 349K 40 wt%	900[a]	$3.13*10^{-10}$	0.4	15.875[c]	31.995	0.1365	$8.98*10^{-10}$	3.4[l]
PI 1M 14 wt%	900[a]	$3.13*10^{-10}$	0.14	45.357[c]	91.414	0.1365	$8.98*10^{-10}$	1[l]
PS 10.2M 6.0 wt%	1070[a]	$3.92*10^{-10}$	0.06	276.667[d]	481.700	0.725[h]	$17.8*10^{-10}$[j]	1[m]
PS 3.9M 10.0 wt%	1070[a]	$3.92*10^{-10}$	0.1	166.000[d]	289.020	0.725[h]	$17.8*10^{-10}$[j]	1[m]

[a] Data taken from [87].
[b] Average over PMA, PEA and POA [82].
[c] The value is given as M_e/φ [81, 79] with M_e = 6.350 kg/mol.
[d] The value is given as M_e/φ [81, 79] with M_e = 16.600 kg/mol.
[e] The values are calculated according to Eq. 16.
[f] The value is taken from [53] considering M_e=6.9 kg/mol.
[g] The value is calculated according to Eq. 19 using m_b=0.064 kg/mol, C_∞=10.2 [87] and $\cos(\theta/2)$=0.83 [82].
[h] The value is calculated according to Eq. 19 using m_b=0.052 kg/mol, C_∞=9.6 [87] and $\cos(\theta/2)$=0.83 [82].
[i] The value is calculated according to Eq. 20 using C_∞=10.2 [87] and $\cos(\theta/2)$=0.83 [82].
[j] The value is calculated according to Eq. 20 using C_∞=9.6 [87] and $\cos(\theta/2)$=0.83 [82].
[k] Data taken from [53] for $M=M_w$.
[l] Data taken from [103] (note that $\zeta_{eq}/\zeta_{aligned}$ for PI were taken from Figure 6 in [103] as maximum values).
[m] No change in $\zeta_{eq}/\zeta_{aligned}$ is considered here.

TABLE III. Molecular weight distribution related parameters taken from [28, 29, 40, 85] (iPP), [87] (PnBA and PI) and [88] (PS).

Sample name	$M=M_w$ (kg/mol)	PDI (-)	x (-)	λ_{max}[b] (-)
iPP 76K	75.85	4.41	3.62	6.0
iPP 64K	63.75	4.35	3.62	6.0
iPP 56K	56.25	3.95	3.62	6.0
PnBA 210K	209.60	≈1	3.4[a]	4.1
PI 145K	145.00	≈1	3.4[a]	6.8
PI 349K 40 wt%	349.00	≈1	3.4[a]	10.8
PI 1M 14 wt%	1050.00	≈1	3.4[a]	18.2
PS 10.2M 6.0 wt%	10200.00	≈1	3.4[a]	19.5
PS 3.9M 10.0 wt%	3900.00	≈1	3.4[a]	15.1

[a] Typical values [76].
[b] The values are calculated according to the Eq. 25.

TABLE IV. Summary of fitting parameters λ_2 and β of the mGNF model, which were identified on steady uniaxial extensional viscosity data for all tested samples. The corresponding parameters A and ξ calculated using Eq.27 and Eq.24, respectively, are also provided here.

Sample name	λ_2 (s)	β (-)	A (Pa.s)	ξ (-)
iPP 76K	$2.884*10^{-7}$	$2.02*10^{-3}$	$2.44*10^{-3}$	$1.12*10^{-1}$
iPP 64K	$2.843*10^{-7}$	$4.12*10^{-3}$	$1.80*10^{-3}$	$1.26*10^{-1}$
iPP 56K	$2.826*10^{-7}$	$5.78*10^{-3}$	$1.33*10^{-3}$	$1.35*10^{-1}$
PnBA 210K	$3.39*10^{-3}$	$1.03*10^{-2}$	$6.28*10^{0}$	$1.51*10^{-1}$
PI 145K	$5.72*10^{-4}$	$2.24*10^{-3}$	$5.62*10^{1}$	$1.14*10^{-1}$
PI 349K 40 wt%	$6.37*10^{-4}$	$4.36*10^{-3}$	$9.85*10^{-1}$	$1.28*10^{-1}$
PI 1M 14 wt%	$5.68*10^{-4}$	$2.11*10^{-2}$	$2.56*10^{-3}$	$1.80*10^{-1}$
PS 10.2M 6.0 wt%	$1.11*10^{-1}$	$7.32*10^{-2}$	$2.49*10^{-2}$	$2.65*10^{-1}$
PS 3.9M 10.0 wt%	$9.55*10^{-3}$	$4.35*10^{-2}$	$1.76*10^{-2}$	$2.21*10^{-1}$

TABLE V. The Rouse reorientation (or stretch) time, τ_R, calculated according to the Eq. 11 for all tested samples.

Sample name	T (°C)	τ_R (s)
iPP 76K	230	$7.74*10^{-6}$[a]
iPP 64K	230	$5.08*10^{-6}$[a]
iPP 56K	230	$4.30*10^{-6}$[a]
PnBA 210K	21.5	$3.00*10^{-2}$
PI 145K	21.5	$1.42*10^{-2}$
PI 349K 40 wt%	21.5	$2.33*10^{-2}$
PI 1M 14 wt%	21.5	$1.18*10^{-2}$
PS 10.2M 6.0 wt%	21.5	$4.96*10^{-1}$
PS 3.9M 10.0 wt%	21.5	$1.60*10^{-1}$

[a] Values are taken from [53].

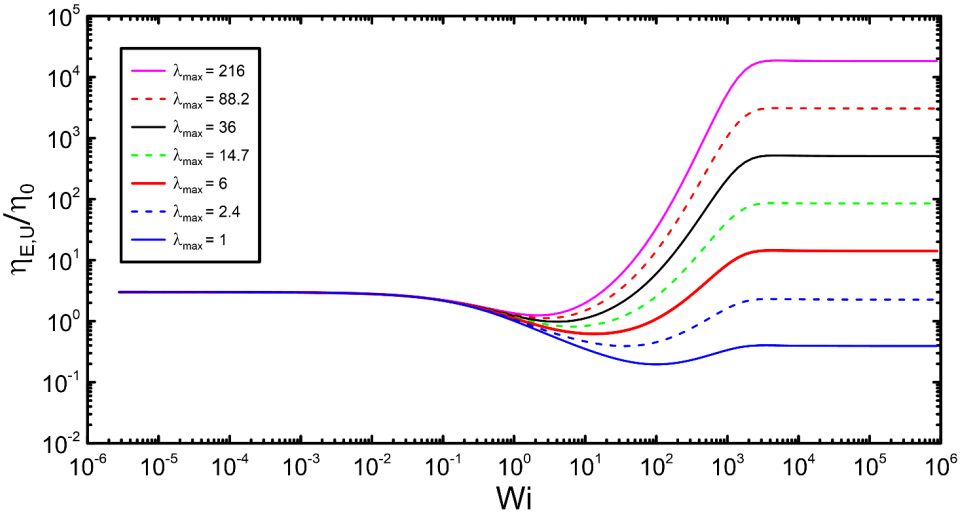

FIG. 1. The uniaxial extensional viscosity, $\eta_{E,U}$, normalized by the zero-shear rate viscosity, η_0, plotted as a function of the orientational Weissenberg number W_i $(=\lambda_1\dot{\varepsilon})$ for different values of λ_{max}. The rheological and molecular constants are considered to be for iPP 76K (see Tables I-III) with $\beta = 10^{-2.5}$, $\lambda_2 = 10^{-7}$ s and $\zeta_{eq}/\zeta_{aligned} = 1$ in this case.

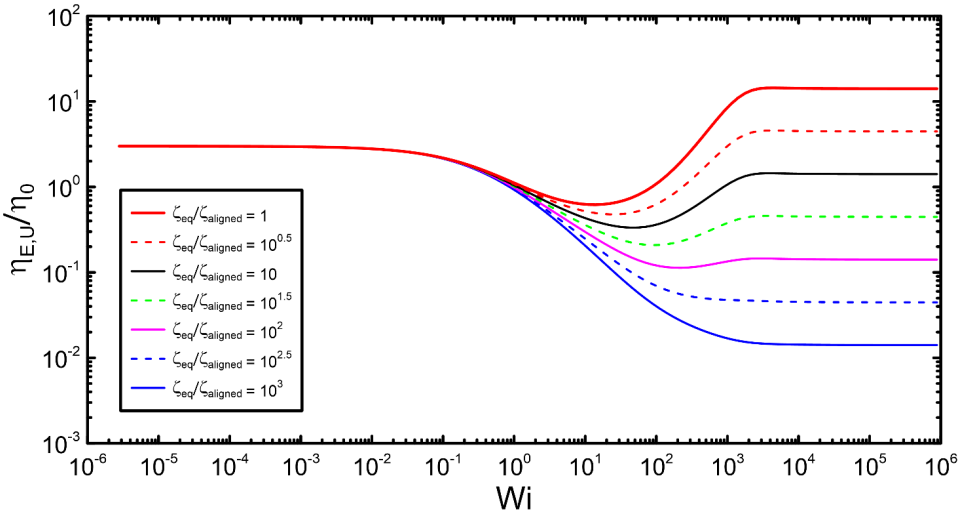

FIG. 2. The uniaxial extensional viscosity, $\eta_{E,U}$, normalized by the zero-shear rate viscosity, η_0, plotted as a function of the orientational Weissenberg number W_i ($=\lambda_1\dot{\varepsilon}$) for different values of the $\zeta_{eq}/\zeta_{aligned}$ ratio. The rheological and molecular constants are considered to be for iPP 76K (see Tables I-III) with $\beta = 10^{-2.5}$, $\lambda_2 = 10^{-7}$ s and $\lambda_{max} = 6$ in this case.

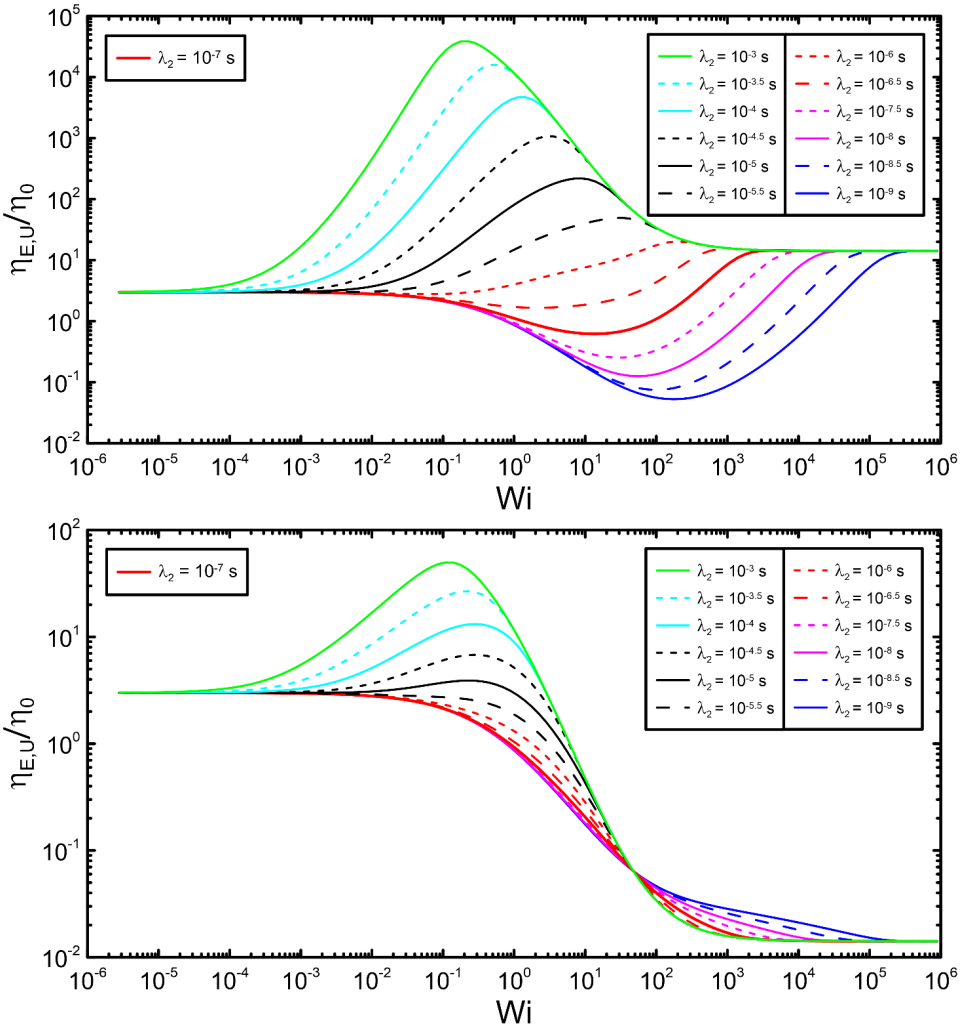

FIG. 3. The uniaxial extensional viscosity, $\eta_{E,U}$, normalized by the zero-shear rate viscosity, η_0, plotted as a function of the orientational Weissenberg number Wi ($=\lambda_1\dot{\varepsilon}$) for different values of the λ_2 with $\zeta_{eq}/\zeta_{aligned}=1$ (top) and $\zeta_{eq}/\zeta_{aligned}=10^3$ (bottom). The rheological and molecular constants are considered to be for iPP 76K (see Tables I-III) with $\beta=10^{-2.5}$ and $\lambda_{max}=6$ in this case.

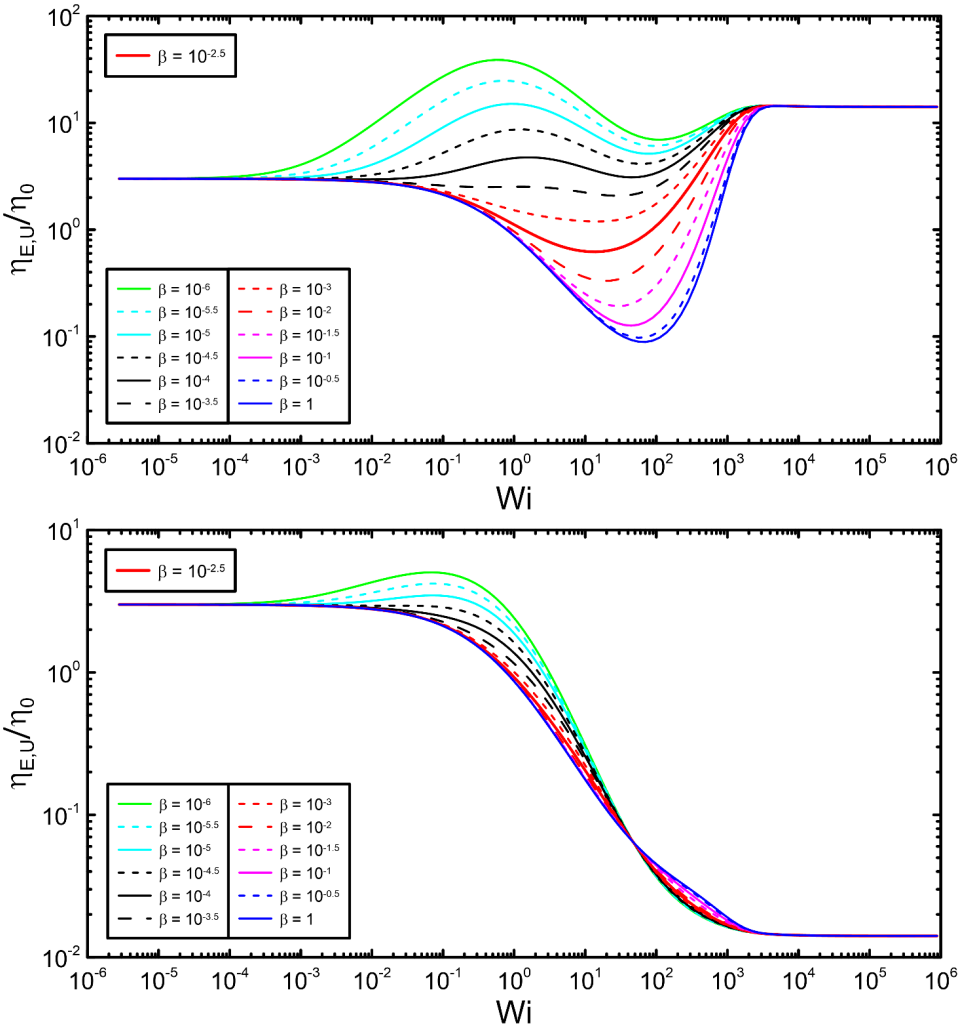

FIG. 4. The uniaxial extensional viscosity, $\eta_{E,U}$, normalized by the zero-shear rate viscosity, η_0, plotted as a function of the orientational Weissenberg number Wi $(=\lambda_1\dot{\varepsilon})$ for different values of the β with $\zeta_{eq}/\zeta_{aligned}=1$ (top) and $\zeta_{eq}/\zeta_{aligned}=10^3$ (bottom). The rheological and molecular constants are considered to be for iPP 76K (see Tables I-III) with $\lambda_2=10^{-7}$ s and $\lambda_{max}=6$ in this case.

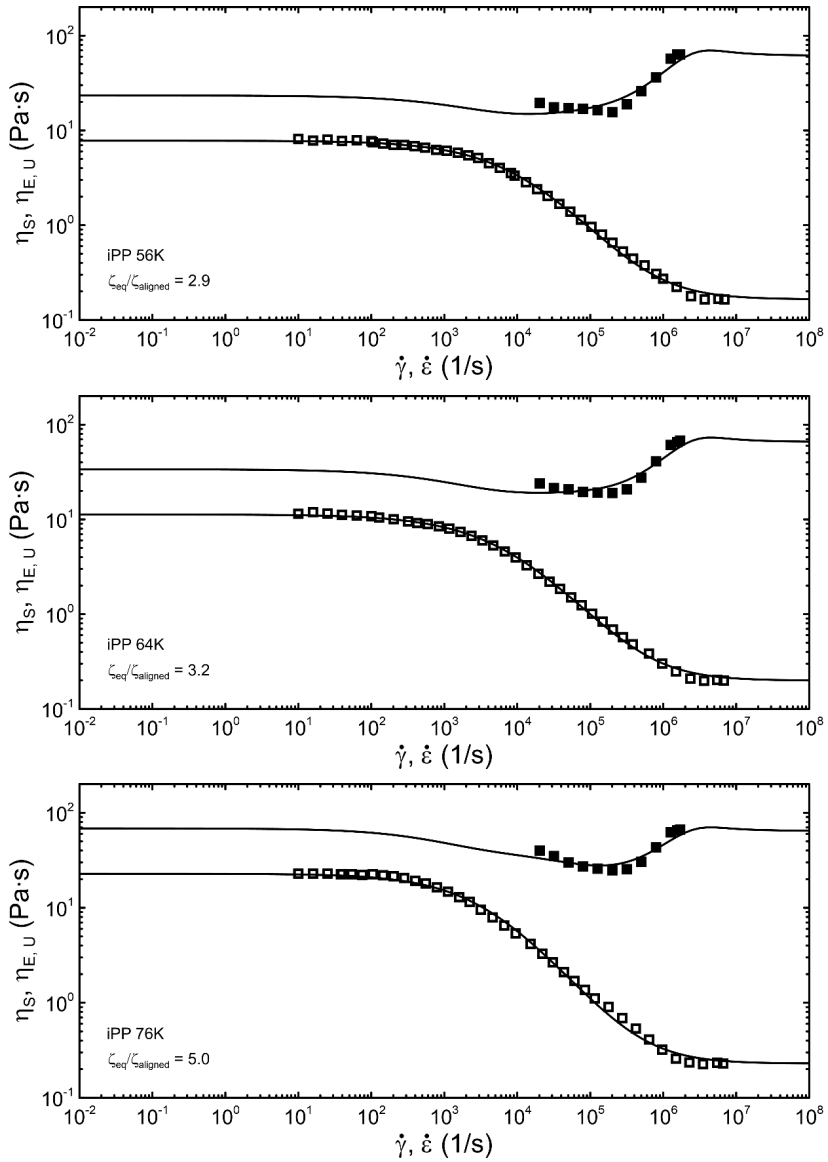

FIG. 5. Comparison between the measured deformation rate dependent shear (open symbols) and uniaxial extensional viscosities (full symbols) and mGNF model fits (curves) for given $\zeta_{eq}/\zeta_{aligned}$ ratios at 230°C for three linear isotactic polypropylenes (iPP 56K – top, iPP 64K – middle, iPP 76K – bottom). Experimental data are taken from [28] and [40]. Here, η_S the shear viscosity, $\eta_{E,U}$, the uniaxial extensional viscosity, $\dot{\gamma}$ the shear rate, $\dot{\varepsilon}$ the extensional strain rate.

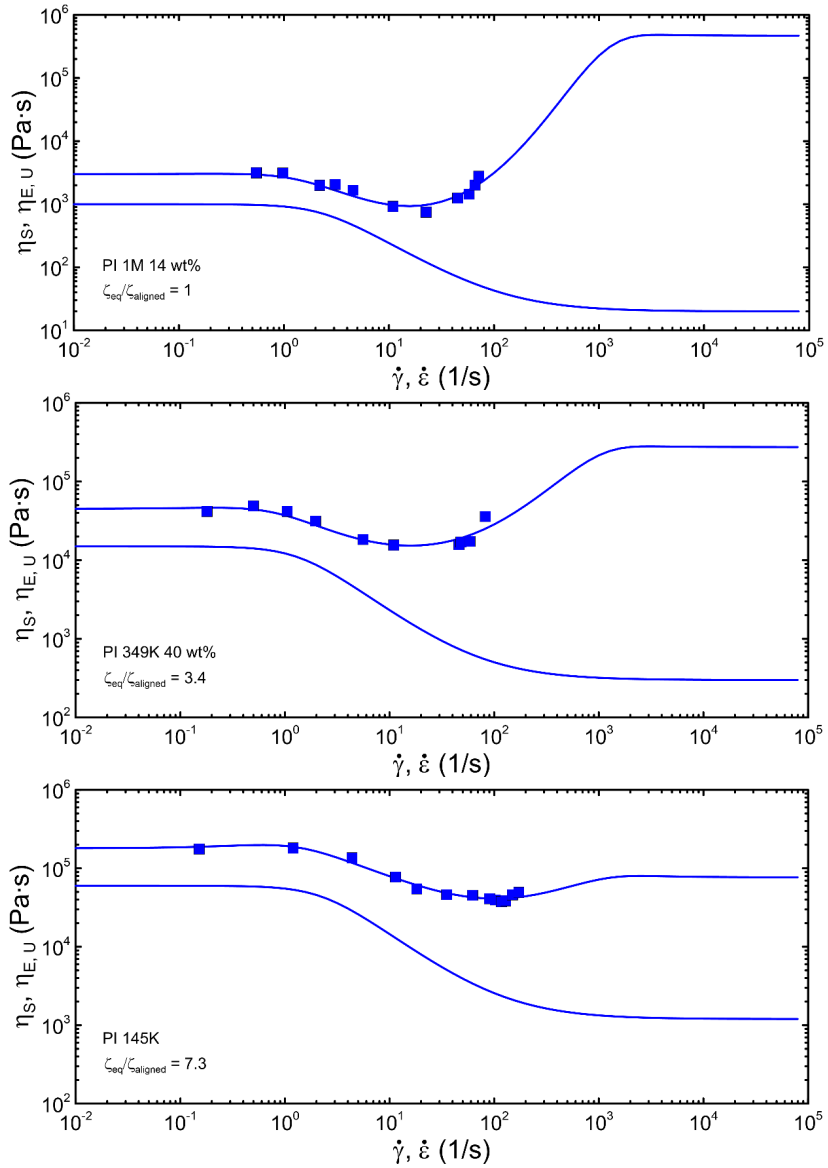

FIG. 6. Comparison between the measured deformation rate dependent uniaxial extensional viscosities (full symbols) and mGNF model fits (upper curves) and shear viscosity predictions (lower curves) for given $\zeta_{eq}/\zeta_{aligned}$ ratios at 21.5ºC for three PI entangled liquids (14 wt% solution – top, 40 wt% solution – middle, melt – bottom). Experimental data are taken from [87]. Here, η_S the shear viscosity, $\eta_{E,U}$, the uniaxial extensional viscosity, $\dot{\gamma}$ the shear rate, $\dot{\varepsilon}$ the extensional strain rate.

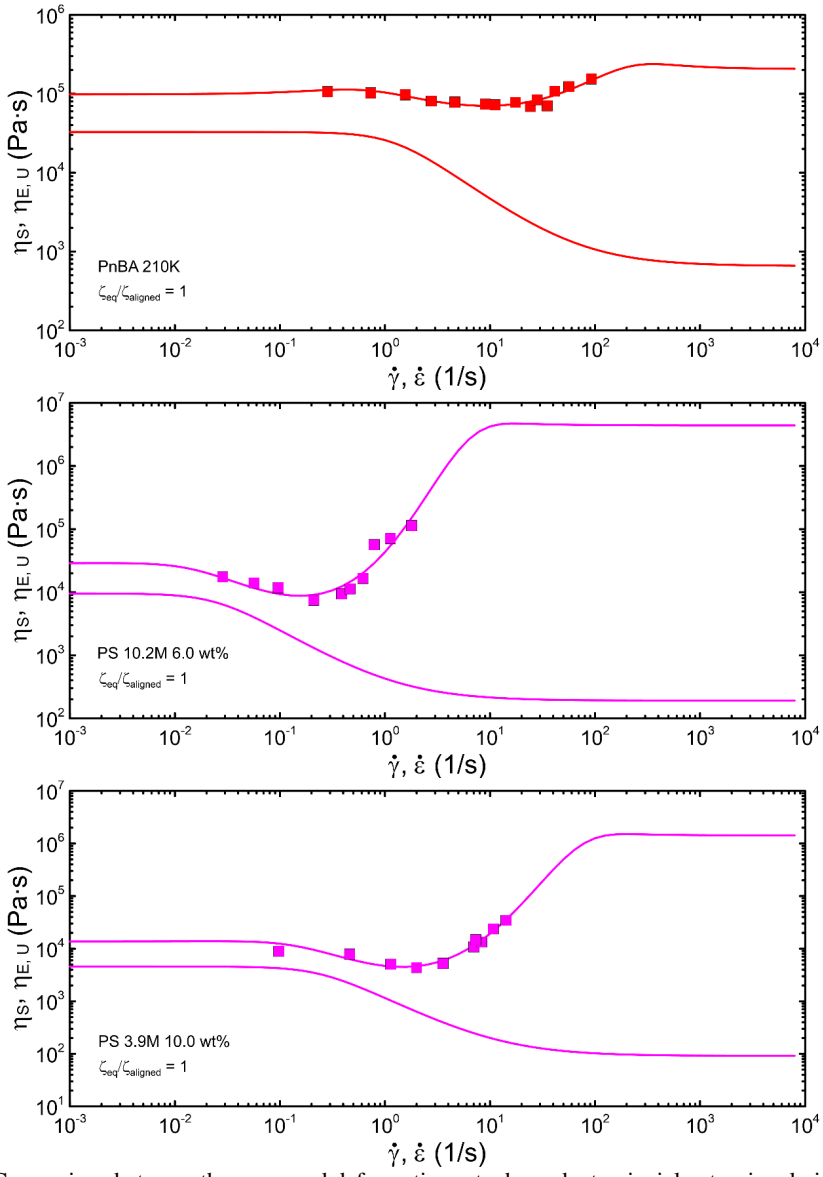

FIG. 7. Comparison between the measured deformation rate dependent uniaxial extensional viscosities (full symbols) and mGNF model fits (upper curves) and shear viscosity predictions (lower curves) at 21.5ºC for three entangled liquids with the same $\zeta_{eq}/\zeta_{aligned}$ ratio (PnBA melt – top, 6 wt% PS solution – middle, 10 wt% PS solution – bottom). Experimental data for PnBA and PS are taken from [87] and [88], respectively. Here, η_S the shear viscosity, $\eta_{E,U}$, the uniaxial extensional viscosity, $\dot{\gamma}$ the shear rate, $\dot{\varepsilon}$ the extensional strain rate.

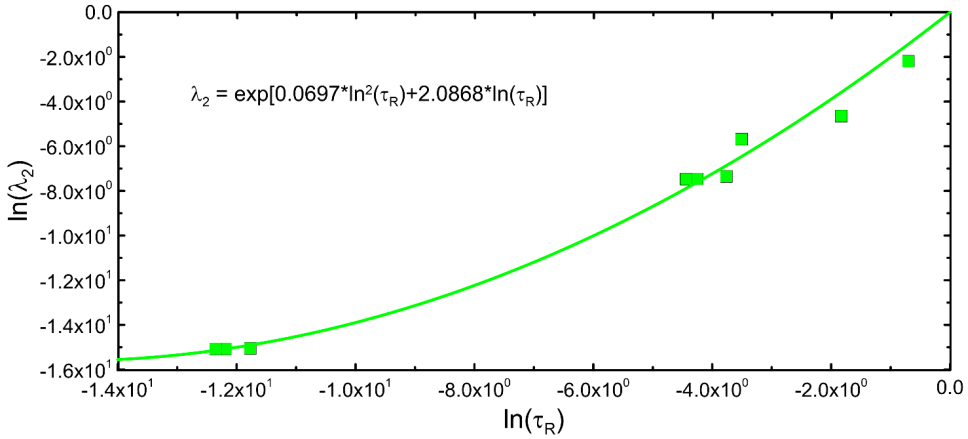

FIG. 8. Relationship between the mGNF model parameter λ_2 and the Rouse reorientation (or stretch) time τ_R for all tested polymer liquids.

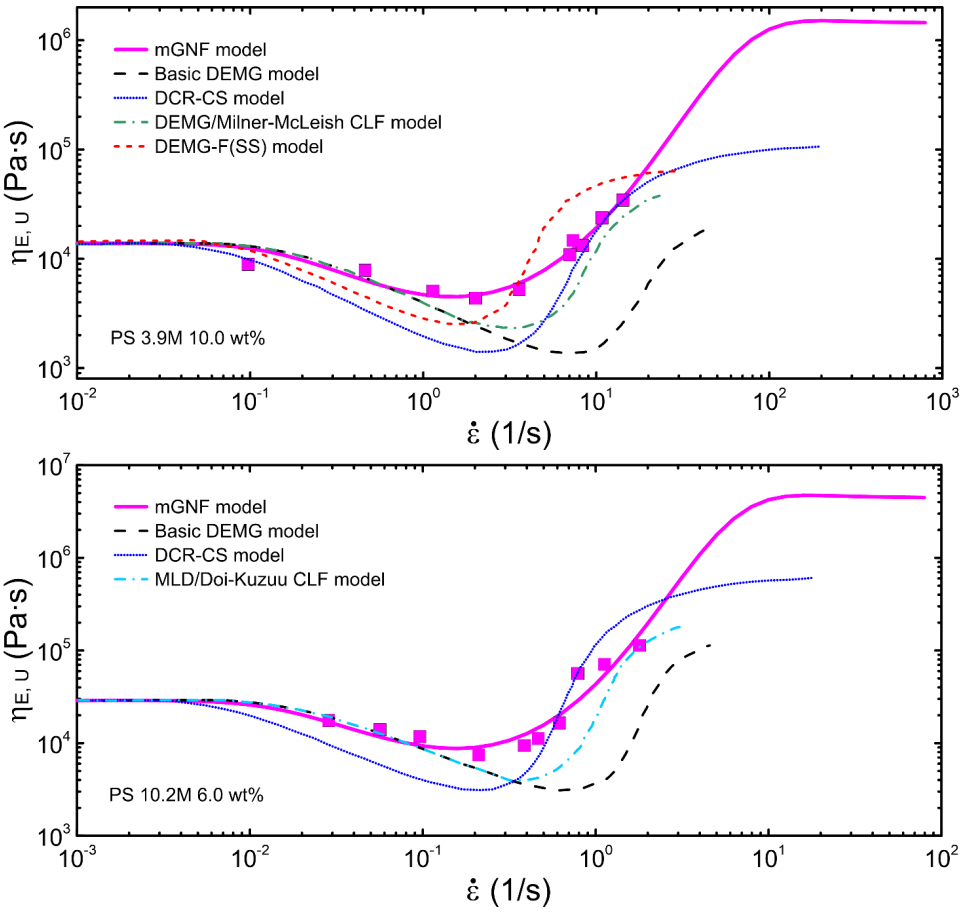

FIG. 9. Comparison between the measured deformation rate dependent uniaxial extensional viscosities (full symbols), mGNF model fits and predictions of different viscoelastic models taken from the open literature (Basic DEMG [88], DEMG/Milner-McLeish CLF [88], MLD/Doi-Kuzuu CLF [88], DCR-CS [104], DEMG-F(SS) [99]) at 21.5ºC for two entangled liquids (10 wt% PS solution – top, 6 wt% PS solution). Experimental data for PS are taken from [88].